

Reasoning and Tool-use Compete in Agentic RL: From Quantifying Interference to Disentangled Tuning

Yu Li¹ Mingyang Yi¹ Xiuyu Li¹ Ju Fan¹ Fuxin Jiang² Binbin Chen² Peng Li³ Jie Song³ Tieying Zhang³

Abstract

Agentic Reinforcement Learning (ARL) focuses on training large language models (LLMs) to interleave reasoning with external tool execution to solve complex tasks. Most existing ARL methods train a single shared model parameters to support both reasoning and tool-use behaviors, implicitly assuming that joint training leads to improved overall agent performance. Despite its widespread adoption, this assumption has rarely been examined empirically. In this paper, we systematically investigate this assumption by introducing a Linear Effect Attribution System (LEAS), which provides quantitative evidence of interference between reasoning and tool-use behaviors. Through an in-depth analysis, we show that these two capabilities often induce misaligned gradient directions, leading to training interference that undermines the effectiveness of joint optimization and challenges the prevailing ARL paradigm. To address this issue, we propose Disentangled Action–Reasoning Tuning (DART), a simple and efficient framework that explicitly decouples parameter updates for reasoning and tool-use via separate low-rank adaptation modules. Experimental results show that DART consistently outperforms baseline methods with averaged 6.35%+ improvements and achieves performance comparable to multi-agent systems that explicitly separate tool-use and reasoning using a single model.

1. Introduction

Recent advances in Agentic Reinforcement Learning (ARL) for post-training (Ouyang et al., 2022; Bai et al., 2022) have substantially extended the capabilities of large language

^{*}Equal contribution ¹School of Information, Renmin University of China, Beijing, China ²Bytedance Inc., Beijing, China ³Bytedance Inc., San Jose, USA. Correspondence to: Mingyang Yi <yimingyang@ruc.edu.cn>, Tieying Zhang <tieying.zhang@bytedance.com>.

models (LLMs). Beyond text generation, modern LLMs can perform complex reasoning and interact with external tools to solve tasks such as information retrieval (Jin et al., 2025), computation (Mai et al., 2025), data analysis (Zhang et al., 2025a), and research workflows (Qiao et al., 2025).

The goal of ARL is to train models that reliably execute external tools while exhibiting strong reasoning abilities (Wu et al., 2024). Most existing ARL paradigms (Schick et al., 2023; Shao et al., 2024; Zeng et al., 2024; Zhang et al., 2025b) jointly optimize these two *heterogeneous capabilities* based on a *single ARL objective with shared model parameters*. This design implicitly assumes that tool execution and logical reasoning can be effectively accommodated within the same parameter space. Whether this assumption consistently holds in practice, however, remains an open question (Wu et al., 2025a; Su et al., 2025).

In this work, we systematically examine this assumption through a controlled empirical analysis of the interaction between tool-use and reasoning capabilities. Specifically, we introduce an **Linear Effect Attribution System** (LEAS), inspired by variance-based frameworks (Greene, 2003), which decomposes an agent’s overall performance into individual capability effects and their interaction terms. By carefully designing control and experimental groups, we show that these capabilities are not independent; instead, they exhibit a clear seesaw phenomenon under joint optimization (Yu et al., 2020). That is, improving tool-use often degrades reasoning, and vice versa. This observation indicates that optimizing both capabilities over shared parameters induces implicit competition, leading to suboptimal performance.

To provide an in-depth analysis of this phenomenon, we examine the optimization dynamics (Ren & Sutherland, 2025; Li et al., 2026) by analyzing gradients induced by different capabilities. We identify a clear gradient conflict, in which gradients associated with tool-use and reasoning tokens are misaligned, causing joint optimization over a shared backbone to update parameters in compromise directions.

Building on this analysis, we propose **Disentangled Action–Reasoning Tuning (DART)**, a framework that assigns separate LoRA (Hu et al., 2022) modules to reasoning and tool-use capabilities. DART freezes the pretrained backbone

and routes reasoning and tool-use tokens to disjoint LoRA adapters. As a result, gradients from the two capabilities are applied to separate parameter subsets, preventing conflicting updates from being applied to the same parameters and thereby mitigating optimization conflicts. We evaluate the DART framework on seven large-scale tool-augmented QA benchmarks. Experimental results show: (1).DART consistently outperforms joint-training baselines across most settings, achieving an average EM score improvement of 6.35%. (2).Compared to specialized multi-agent systems that explicitly separate tool-use and reasoning into different models, DART achieves comparable performance while using a single model.

Our contributions are summarized as follows:

- For ARL training, we empirically identify a negative interaction between tool-use and reasoning capabilities using a Linear Effect Attribution System (LEAS), and show that this interaction is attributed to gradient conflicts under joint training.
- We propose DART, a framework that structurally disentangle gradient for reasoning and tool-use and consistently improves performance on complex agent tasks.
- Extensive experiments show that DART consistently improves performance through training-time disentanglement, achieving averaged 6.35%+ performance improvements compared to baseline method.

2. Related Work

ARL with Tool-use. ARL research focuses on fine-tuning LLMs as autonomous agents that learn to invoke external tools through environment feedback, bridging the gap between reasoning and action without dense step-level supervision tuning (Schick et al., 2023). Recent advancements have optimized various components of this pipeline, including reward formulation to induce emergent behaviors (Qian et al., 2025; Peiyuan et al., 2024; Mai et al., 2025), policy refinement for precise action interleaving (Feng et al., 2025; Singh et al., 2025; Wei et al., 2025), and large-scale trajectory synthesis (Dong et al., 2025; Li et al., 2025a) for scalable training (Jiang et al., 2025). However, none of these existing methods explore the interference between reasoning and tool-use and ensure that they do not hurt the performance of each other as we did.

Multi-LoRA. This approach attaches multiple LoRA adapters to a shared backbone, enabling different adapters to be activated based on specific routing conditions or tasks. Router-driven methods employ learned routers to dynamically select among multiple adapters, aiming to expand effective model capacity through expert specialization (Li et al., 2024; Luo et al., 2024; Zhu et al., 2023; Wu et al., 2025b; Luo et al., 2025). However, the interference between

different abilities can not be disentangled in this regime. In contrast to these methods rely on soft expert mixing, DART disentangles the interference within a single ARL task by explicitly isolating reasoning and tool-use updates into disjoint parameter subspaces. Moreover, unlike task-specific methods (Huang et al., 2024; Wang et al., 2024; Ma et al., 2024), which combine a task-specific LoRA adapter to handle the overall tokens in one task. Our DART assigns different LoRA adapters to each token in one task, which provides more capacity of model.

3. Preliminaries

This section presents the Agentic Reinforcement Learning (ARL) and describes low-rank adaptation (LoRA).

3.1. Agentic Reinforcement Learning

An LLM agent $\pi_\theta(c_t | c_{<t})$ generates a trajectory τ for a query q , interleaving reasoning and tool-use tokens.

$$\tau = (c_1, \dots, c_t, \dots, c_T), \quad (1)$$

To distinguish the functional roles of tokens within this sequence, we define a *role-based* router function $\ell : \{1, \dots, T\} \rightarrow \{r, a\}$. Here, $\ell(t) = r$ indicates that c_t is a **reasoning token**, while $\ell(t) = a$ indicates a **tool-use token**. An illustrative routing case is shown in Figure. 7(B). The agent is optimized to maximize the expected reward $\mathcal{J}(\theta) = \mathbb{E}[R(\tau)]$. We estimate the policy gradient:

$$\nabla_\theta \mathcal{J}(\theta) \approx \mathbb{E}_{\tau \sim \pi_\theta} \left[\mathcal{A}(\tau) \sum_{t=1}^T \nabla_\theta \log \pi_\theta(c_t | c_{<t}) \right]. \quad (2)$$

where $\mathcal{A}(\tau)$ is the advantage derived by reward $R(\tau)$. In standard ARL, a single set of shared parameters θ is updated using gradients from both reasoning and tool-use tokens, without considering the distinction specified by $\ell(t)$.

3.2. Low-Rank Adaptation (LoRA)

To reduce fine-tuning overhead, Low-Rank Adaptation (LoRA) freezes the pre-trained weights $W \in \mathbb{R}^{d \times k}$ and introduces trainable low-rank decomposition matrices. For a given layer, let $\mathbf{h}_t \in \mathbb{R}^k$ denote the hidden state corresponding to token c_t . The forward pass is modified as:

$$\mathbf{h}'_t = W\mathbf{h}_t + \Delta W\mathbf{h}_t = W\mathbf{h}_t + B\mathbf{A}\mathbf{h}_t, \quad (3)$$

where $B \in \mathbb{R}^{d \times r}$ and $A \in \mathbb{R}^{r \times k}$ are low-rank matrices with $r \ll \min(d, k)$. During training, only A and B are updated while W_0 is frozen. LoRA applies the same adapter ΔW to all tokens in trajectory τ .

4. Linear Effect Attribution System

In this section, we investigate whether jointly optimizing reasoning and tool-use in ARL leads to interference between

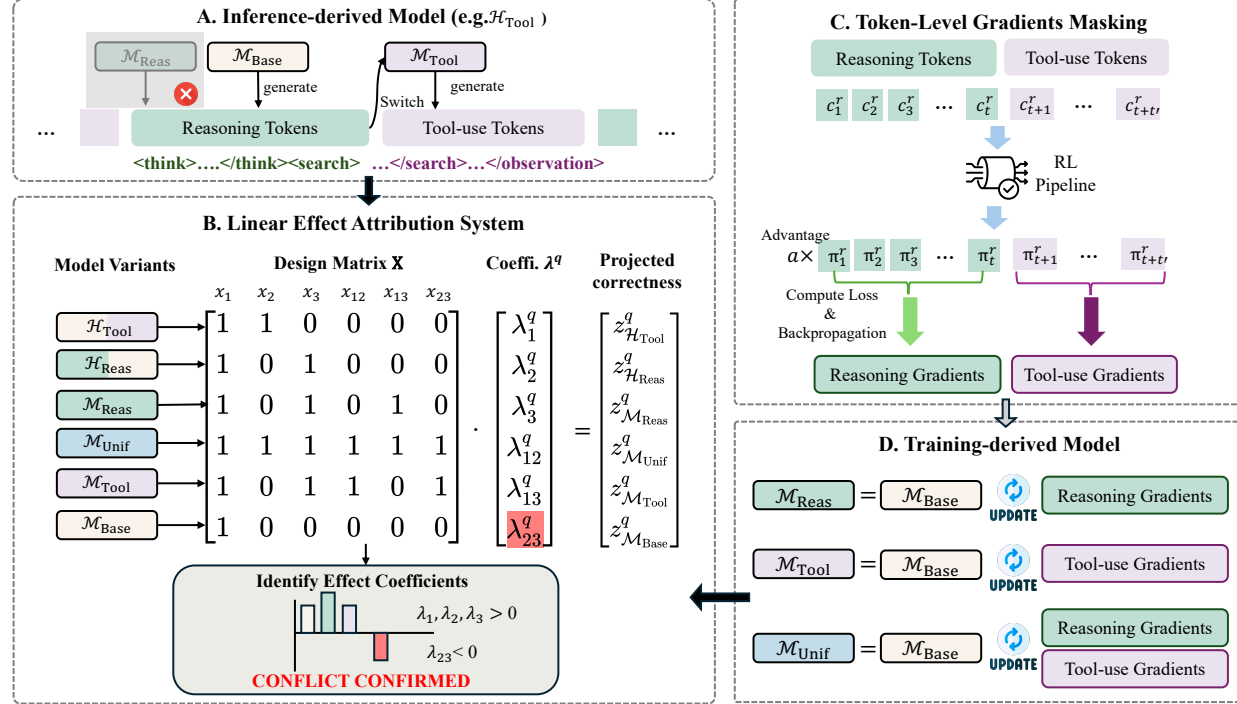


Figure 1. Overview of the Linear Effect Attribution System (LEAS). **(A).Inference-derived Model:** By routing specific token types to different models at inference time, we synthesize capability combinations without parameter-level interaction. **(B).Linear Effect Attribution System:** The six model variants (train-derived and inference-derived) populate the design matrix \mathbf{X} . Solving the linear system yields question-specific coefficients λ^q , where $\lambda_{23} < 0$ signals capability interference. **(C).Token-Level Gradient Masking:** During training, token-level masks selectively route gradients to reasoning or tool-use parameters, isolating capability-specific updates. **(D).Training-derived Models:** This produces specialized model variants derived from a shared backbone, enabling controlled comparisons across different capability combinations.

these capabilities, as hypothesized in Section 1. To this end, we introduce the *Linear Effect Attribution System* (LEAS), a diagnostic framework that isolates the contributions of reasoning and tool-use and explicitly quantifies their interaction. Our analysis reveals a clear **negative interaction**, and further shows that this interference is driven by gradient conflicts during training (Figure 3).

4.1. Formulation of LEAS

In this subsection, we formalize the effect of joint optimization by introducing a set of binary indicators that encode individual capabilities and their pairwise interactions.

Definition 4.1. We characterize an agent’s capability using three binary indicators: base x_1 , tool-use x_2 , reasoning x_3 .

Definition 4.2. To capture potential interference, pairwise interaction indicators $x_{ij} = 1$ when capabilities i and j are jointly optimized, and 0 otherwise.

Based on the above definition, each model \mathcal{M} associates a binary *capability indicator vector*

$$\mathbf{x}_{\mathcal{M}} = [x_1, x_2, x_3, x_{12}, x_{13}, x_{23}] \in \{0, 1\}^6. \quad (4)$$

For example, a model jointly trained for tool-use and reasoning, its capability indicator vector is represented by

$\mathbf{x} = [1, 1, 1, 1, 1, 1]$, reflecting that all individual capabilities and their pairwise interactions are active.

By representing each model with a fixed binary capability vector, we can perform controlled comparisons by comparing different models on the same question.

Assumption 4.3. Let $s_{\mathcal{M}}^q \in (0, 1)$ be the expected correctness of model \mathcal{M} on question q . We model this probability using the capability indicator vector $\mathbf{x}_{\mathcal{M}}$:

$$s_v^q = \sigma(\mathbf{x}_{\mathcal{M}}^\top \boldsymbol{\lambda}^q), \quad \boldsymbol{\lambda}^q = [\lambda_1^q, \lambda_2^q, \lambda_3^q, \lambda_{12}^q, \lambda_{13}^q, \lambda_{23}^q], \quad (5)$$

Here $\sigma(\cdot)$ is the sigmoid function, while λ_i^q and λ_{ij}^q are the main and interaction effects for question q .

As can be seen, for the parameters of interaction terms, $\lambda_{ij}^q > 0$ indicates synergy and $\lambda_{ij}^q < 0$ indicates interference. Thus, to identify the existence of interference is equivalent to checking the sign of λ .

Remark 4.4. While Eq. 5 resembles logistic regression, it is employed for *attribution rather than prediction*. Our goal is not to model absolute probabilities, but to identify the **sign** of interaction coefficients λ_{ij}^q —specifically, to distinguish between synergy ($\lambda_{ij}^q > 0$) and interference ($\lambda_{ij}^q < 0$).

Identify effect coefficients λ^q . We apply the logit transform

to Eq. 5 to convert the model into a linear equation:

$$z_{\mathcal{M}}^q = \log \frac{s_{\mathcal{M}}^q}{1 - s_v^q} = \mathbf{x}_{\mathcal{M}}^\top \boldsymbol{\lambda}^q, \quad (6)$$

Each model \mathcal{M} provides a linear equation via $\mathbf{x}_{\mathcal{M}}$. Stacking these from multiple models yields the linear equations system used to solve for $\boldsymbol{\lambda}$:

$$\mathbf{z}^q = \mathbf{X} \boldsymbol{\lambda}^q, \quad (7)$$

where \mathcal{M} -th row of *design matrix* \mathbf{X} corresponds to $\mathbf{x}_{\mathcal{M}}$. To uniquely identify $\boldsymbol{\lambda}^q \in \mathbb{R}^6$, we should employ six models with **linearly independent** capability indicator vectors.

4.2. Constructing Model via Gradient Mask Training and Hybrid Inference

We next describe how we construct a set of model variants used in LEAS to analyze the interaction between reasoning and tool-use. These models populate the design matrix \mathbf{X} shown in Fig. 1B. To this end, we employ a two-stage strategies starting from a common base model. Firstly, we obtain three training-based models by applying **gradient masking**. Secondly, we synthesize two inference-derived models via constructed **hybrid inference** processes. We now describe each model in detail.

4.2.1. BASE MODEL AND TRAINING-DERIVED MODELS.

As shown in Fig. 1D, we first construct three training-derived models starting from a common base model. To this end, we need a pretrained model as the base model.

1. Base Model $\mathcal{M}_{\text{Base}}$. The base model is the off-the-shelf pretrained LLM before applying any of tool-use or reasoning-specific post-training. It serves as the base model that provides fundamental capabilities. Accordingly, only the base capability indicator is active, yielding $\mathbf{x}_{\text{Base}} = [1, 0, 0, 0, 0, 0]$.

Building upon this base model, we construct three training-derived models via **gradient masking** technique to isolate the captured capability during training. Notably, the training data, model architecture, and optimization hyper-parameters are kept identical to ensure consistency across all backbones.

Based on the definition of token type $\ell(t)$ in Section 3, we define a binary mask sequence $\mathbf{m} = [m_1, \dots, m_T]$ to selectively isolate parameter updates. Concretely, we make the gradient of the RL objective in Eq.(2) becomes:

$$\nabla_{\theta} \mathcal{J}(\theta) \approx \mathbb{E}_{\tau \sim \pi_{\theta}} \left[\sum_{t=1}^T \nabla_{\theta} \log \pi_{\theta}(c_t | c_{<t}) \cdot \mathcal{A}(\tau) \cdot m_t \right], \quad (8)$$

where $m_t \in \{0, 1\}$ acts as a gate controlling whether the gradient from token c_t contributes to the update.

To systematically define these gates, we partition the trajectory indices $\{1, \dots, T\}$ into two disjoint sets based on the

label function $\ell(t)$:

$$\mathcal{T}_{\text{reas}} = \{t \mid \ell(t) = r\}, \quad \mathcal{T}_{\text{tool}} = \{t \mid \ell(t) = a\}. \quad (9)$$

These sets correspond to the tokens associated with reasoning and tool-use capabilities, respectively.

Let $\mathbb{I}(\cdot)$ denote the indicator function. Then, with all these definitions, we are ready to introduce our three training-derived models derived by different masking schemes 2.

Reasoning-specialized model $\mathcal{M}_{\text{Reas}}$. We define gradient mask

$$m_t^{(\text{Reas})} = \mathbb{I}(t \in \mathcal{T}_{\text{reas}}).$$

By plugging this gradient mask into Eq.(8) we obtain a model with reasoning capability while without the tool-use capability. Then, the model corresponds to a capability indicator vector is $\mathbf{x}_{\text{Reas}} = [1, 0, 1, 0, 1, 0]$.

3. Tool-specialized model $\mathcal{M}_{\text{Tool}}$. Similarly, we define the gradient mask

$$m_t^{(\text{Tool})} = \mathbb{I}(t \in \mathcal{T}_{\text{tool}}),$$

and plug it into (2). Then we obtain a model with tool-use capability but without altering its reasoning behavior. The corresponding capability indicator vector is $\mathbf{x}_{\text{Tool}} = [1, 1, 0, 1, 0, 0]$.

4. Unified model $\mathcal{M}_{\text{Unified}}$. Finally, we define the gradient mask

$$m_t^{(\text{Uni})} = 1, \quad \forall t \in \{1, \dots, T\},$$

which corresponds to the standard ARL training setting with a capability indicator vector $\mathbf{x}_{\text{Unified}} = [1, 1, 1, 1, 1, 1]$.

4.2.2. INFERENCE-DERIVED MODEL.

With the aforementioned models as backbones, we can construct the remaining two models via hybrid inference processes. Concretely, as shown in Fig. 1A, hybrid inference is an inference-time composition scheme that routes different token types to different trained models. We construct two inference-derived models as follows:

5. Tool-hybrid model $\mathcal{H}_{\text{Tool}}$. We use the base model $\mathcal{M}_{\text{Base}}$ for reasoning, while the tool-specialized model $\mathcal{M}_{\text{Tool}}$ is invoked exclusively for tool-action tokens. Since these capabilities are composed at inference time instead of jointly optimized, no parameter-level interaction is introduced between base and tool-use capabilities. Thus, all interaction indicators involving tool-use are zero, yielding $\mathbf{x}_{\mathcal{H}_{\text{Tool}}} = [1, 1, 0, 0, 0, 0]$.

6. Reasoning-hybrid model $\mathcal{H}_{\text{Reas}}$. Similarly, we use the reasoning specialized model $\mathcal{M}_{\text{Reas}}$ for reasoning tokens, and the base model $\mathcal{M}_{\text{Base}}$ to handle tool-action tokens. No jointly optimized parameter are introduced between the base and reasoning capabilities, so that the corresponding capability indicator vector is $\mathbf{x}_{\mathcal{H}_{\text{Reas}}} = [1, 0, 1, 0, 0, 0]$.

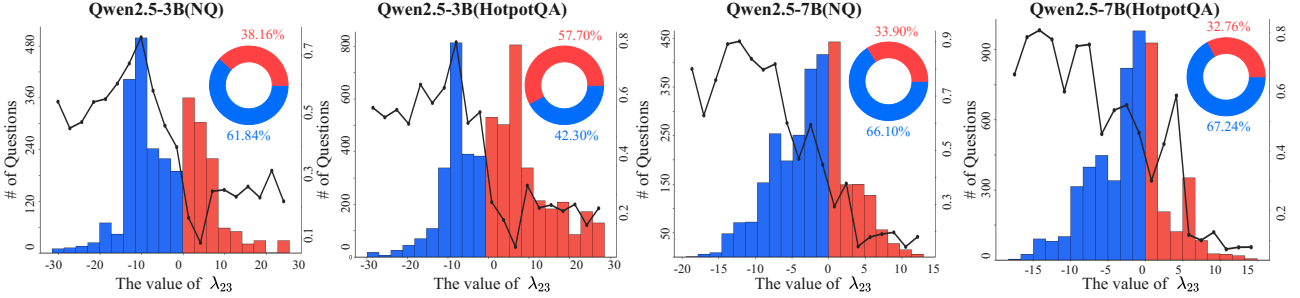


Figure 2. Interaction between reasoning and tool-use under ARL. Histograms show the distribution of the question-level interaction coefficient λ_{23}^q on NQ and HotpotQA using Qwen2.5-Instruct models (3B and 7B), where negative values (blue) indicate interference and positive values (red) indicate synergy. The overlaid curve shows ARL accuracy averaged over questions within each λ_{23}^q bin.

As summarized in Fig. 1B, by ensuring the linear independence of the rows in the design matrix \mathbf{X} (corresponding to the six models), we guarantee the identifiability of the effect coefficients $\boldsymbol{\lambda}^q$ used for diagnosing capability interactions.

4.3. Empirical Analysis

Reasoning-Tool Interaction. Following (Jin et al., 2025), we instantiate LEAS on NQ and HotpotQA datasets to study the interaction coefficient λ_{23}^q between two capabilities.

For each question q , we solve for $\boldsymbol{\lambda}^q$ using the design matrix \mathbf{X} induced by the six model variants defined in Section 4.2. All training-derived models are trained under identical hyper-parameters and to convergence. The correctness s_v^q of question q is estimated via 50 stochastic samples per model-question pair. Additional implementation details are provided in Appendix D.

Fig. 2 presents the distribution of the interaction coefficient λ_{23}^q together with the average correctness aggregated over all six models. As can be seen, for most questions, the interference happen i.e., $\lambda_{23}^q < 0$. Moreover, these questions achieve markedly higher accuracy than those in the synergy region.

These results show that **ARL predominantly succeeds in the interference region** ($\lambda_{23}^q < 0$). This observation supports our hypothesis that joint optimization over shared parameters induces implicit competition between capabilities and leads to sub-optimal outcomes compared to independent learning. Besides that, the higher accuracy indicates that solving tasks correctly requires using both skills at the same time, which naturally increases the conflict when they compete for the same shared parameters.

Gradient Conflict. Finally, let us make an explanation to the interference. Following the training settings described by (Jin et al., 2025), we analyze the relationship between the gradient of reasoning and tool-use, by comparing the angles of their gradients. Based on Eq. 8, we compute the gradient $\mathbf{g}_\tau^{(b)}$ for token type $b \in \{r, a\}$ in trajectory τ across

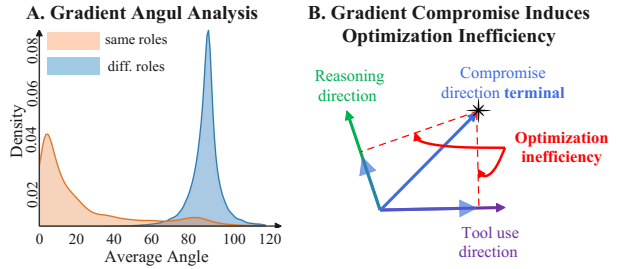


Figure 3. Gradient misalignment leads to optimization inefficiency. (A). Gradient angle distributions on NQ under Qwen2.5-3B, where same-capability gradients are aligned, while reasoning and tool-use gradients are nearly orthogonal. (B). Averaged orthogonal gradients yield a compromise update direction, leading to optimization inefficiency.

$N = 16$ rollouts. We calculate the average angle between gradients of the different roles within the same trajectory $\mathbb{E}_i[\angle(\mathbf{g}_{\tau_i}^{(r)}, \mathbf{g}_{\tau_i}^{(a)})]$. Moreover, to create a baseline, we calculate the average angle between gradients of the same role (e.g., reasoning-to-reasoning) from different trajectories $\mathbb{E}_{i \neq j}[\angle(\mathbf{g}_{\tau_i}^{(b)}, \mathbf{g}_{\tau_j}^{(b)})]$. Additional implementation details are provided in Appendix E.

As shown in Fig. 3, the angles between same-type gradients are small, while the gradients in different types (reasoning and tool-use) are nearly orthogonal.

This orthogonality indicates that *each task has its own distinct optimal update direction*. Consequently, joint optimization that averages these gradients forces the update toward a **compromise direction**. This direction is sub-optimal for both reasoning and tool-use, leading to a fundamental optimization bottleneck that limits the ARL potential.

5. Disentangled Action-Reasoning Tuning

The analysis in Figure 2 reveals a systematic negative interaction between tool-use and reasoning under joint optimization, arising from conflicting gradient updates in a shared parameter space (Figure 3).

To mitigate this issue, we propose an *explicit gradient isola-*

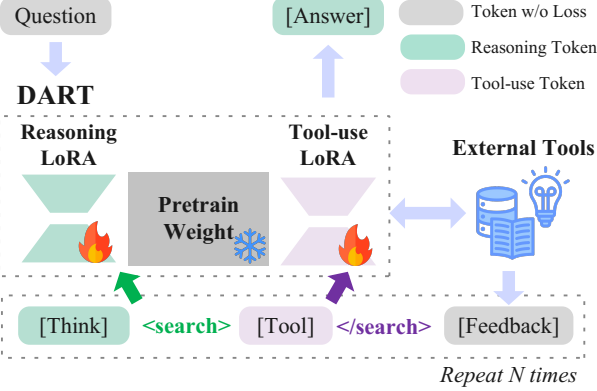


Figure 4. **Illustration of DART.** A frozen backbone augmented with two disjoint LoRA adapters for reasoning and tool-use, both attached to all linear layers, where a token-level router directs gradients into separate parameter subspaces to avoid interference.

tion mechanism between tool-use and reasoning. Intuitively, this can be done by isolating the gradient from tool-use exclusively update the tool parameter, while the gradients from reasoning are applied to the reasoning parameters.

A straightforward solution is to train two independent models (2-Agent systems), but this approach doubles storage and deployment overhead (see Appendix F for details). To avoid this overhead, we propose **Disentangled Action-Reasoning Tuning (DART)**, which freezes the pretrained backbone weights W and introduces two disjoint LoRA adapters: $\theta^r = \{B_r, A_r\}$ for reasoning and $\theta^a = \{B_a, A_a\}$ for tool-use. This design enables token-level routing over a shared backbone during decoding.

With this architecture, at each decoding step t , the model activates an adapter $u_t \in r, a$ determined by the token router $\ell(t)$ (Section 3). As illustrated in Figure 4, token roles are partitioned by special tokens (e.g., `<search>` triggers tool-use LoRA). Consequently, the forward pass for the hidden state \mathbf{h}_t is computed as:

$$\mathbf{h}'_t = W\mathbf{h}_t + B_{u_t}A_{u_t}\mathbf{h}_t. \quad (10)$$

As each token activates only the adapter associated with its capability type, the two parameter sets θ^r and θ^a are updated independently. Since tool-use and reasoning are never jointly optimized in DART, the interaction indicator defined in Section 4.1 satisfies $x_{23} = 0$. As a result, the corresponding interaction term is never activated in LEAS, and the associated coefficient λ_{23} is effectively zero.

Remark 5.1. We freeze the backbone W to enforce gradient isolation; otherwise, gradients from reasoning and tool-use tokens would update shared parameters, undermining disentanglement. Importantly, *freezing the backbone does not sacrifice performance*: recent studies show that RL-based tuning primarily affects sparse subnetworks (Mukherjee et al., 2025), and that LoRA can match full-parameter

performance (Schulman & Lab, 2025). Unlike MoE architectures, where soft expert mixing still allows interference between capabilities, DART enforces strict disentanglement by directing reasoning and tool-use updates to separate parameter subspaces.

6. Experiments

Following Search-R1 (Jin et al., 2025), we empirically evaluate DART on large-scale tool-augmented QA benchmarks to check whether it improves the overall performance of post-trained model in tool using scheme, and mitigates the interference between tool using and reasoning.

Datasets. We evaluate on seven benchmarks categorized into two settings: **General QA** includes Natural Questions (NQ) (Kwiatkowski et al., 2019), TriviaQA (Joshi et al., 2017), and PopQA (Mallen et al., 2022), which primarily assesses *factual retrieval* and *single-step QA capabilities*. **Multi-Hop QA** includes HotpotQA (Yang et al., 2018), 2WikiMultiHopQA (Ho et al., 2020), Musique (Trivedi et al., 2022), and Bamboogle (Press et al., 2023), which require composing evidence *across multiple documents and reasoning steps*.

Experimental Setup. Unless otherwise stated, all experiments use the same backbone, tool stack, and training pipeline to ensure fair comparisons. Detailed hyperparameters are provided in Appendix B.

During training stage, we merge the training splits of **NQ** and **HotpotQA** to form a unified dataset for all fine-tuning/RL-based baselines. All evaluations are conducted on the official test (or validation) splits of seven QA benchmarks to measure both **in-domain** performance and **out-of-domain** generalization. Following (Yu et al., 2024), we report **Exact Match (EM)** as the primary metric.

6.1. Main Results

In this section, we present the comprehensive evaluation of DART to see its performance on benchmark datasets. We compare it against a diverse set of baselines across multiple model scales to verify its performance and stability on both General and Multi-Hop QA tasks.

Baselines. The baselines are categorized into three types: (1) **Standard Inference**: Including Direct Inference and Chain-of-Thought (CoT) reasoning (Wei et al., 2022) and Rejection Sampling (Ahn et al., 2024). (2) **Tool-Augmented Inference**: Methods that integrate external knowledge, including IRCoT (Trivedi et al., 2023), RAG (Lewis et al., 2020), Search-o1 (Li et al., 2025b), and Search-R1 (Jin et al., 2025). (3) **Post-training**: Strong baselines involving supervised fine-tuning(SFT) (Chung et al., 2024), R1 variants (base/instruct) (Guo et al., 2025).

As shown in Tables 1 and 2, DART consistently achieves substantial gains across all settings. (1) The improvements

Table 1. Results on General QA and Multi-Hop QA datasets for **Qwen2.5-3b-Base/Instruct**. The best performance is set in bold. \diamond denotes results from (Jin et al., 2025). \dagger denotes in-domain datasets and $*$ denotes out-domain datasets.

Methods	General QA			Gen-Avg	Multi-Hop QA				MH-Avg	Avg
	NQ \dagger	TriviaQA*	PopQA*		HotpotQA \dagger	2Wiki*	Musique*	Bamboogle*		
Direct Inference \diamond	0.106	0.288	0.108	0.167	0.149	0.244	0.020	0.024	0.109	0.134
CoT \diamond	0.023	0.032	0.005	0.020	0.021	0.021	0.002	0.000	0.011	0.015
IRCoT \diamond	0.111	0.312	0.200	0.208	0.164	0.171	0.067	0.240	0.161	0.181
Search-o1 \diamond	0.238	0.472	0.262	0.324	0.221	0.218	0.054	0.320	0.203	0.255
RAG \diamond	0.348	0.544	0.387	0.426	0.255	0.226	0.047	0.080	0.152	0.270
SFT \diamond	0.249	0.292	0.104	0.215	0.186	0.248	0.044	0.112	0.147	0.176
R1-base \diamond	0.226	0.455	0.173	0.285	0.201	0.268	0.055	0.224	0.187	0.229
R1-instruct \diamond	0.210	0.449	0.171	0.277	0.208	0.275	0.060	0.192	0.184	0.224
Rejection Sampling \diamond	0.294	0.488	0.332	0.371	0.240	0.233	0.059	0.210	0.186	0.265
Search-R1-PPO-Base \diamond	0.406	0.587	0.435	0.476	0.284	0.273	0.049	0.088	0.174	0.303
Search-R1-PPO-Ins \diamond	0.341	0.545	0.378	0.421	0.324	0.319	0.103	0.264	0.253	0.325
Qwen2.5-3b-Instruct										
Search-R1-GRPO \diamond	0.397	0.565	0.391	0.451	0.331	0.310	0.124	0.232	0.249	0.336
DART	0.451	0.602	0.476	0.510	0.392	0.376	0.143	0.352	0.316	0.399
Qwen2.5-3b-Base										
Search-R1-GRPO \diamond	0.440	0.582	0.413	0.478	0.265	0.244	0.061	0.113	0.171	0.303
DART	0.457	0.605	0.478	0.513	0.399	0.389	0.155	0.352	0.324	0.405

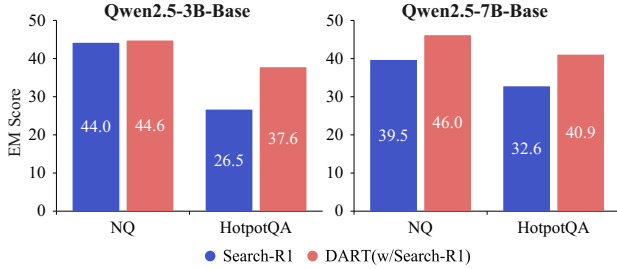


Figure 5. **Reasoning under Fixed Retrieval.** DART achieves higher EM than Search-R1 on NQ and HotpotQA when both use identical retrieval contexts, demonstrating improved reasoning capability independent of retrieval quality.

hold for both in-domain and out-of-domain datasets, with notable gains on HotpotQA and Bamboogle for the 3B-Base model, indicating that *DART learns a robust tool-use strategy rather than overfitting to specific training patterns.* (2) DART yields larger gains on Multi-Hop QA than on general QA, improving the 3B-Base model’s average score from 0.171 to 0.324. We speculate the improvement is because the Multi-Hop QA requires tight coordination between tool-use and reasoning, the *disentangled two capabilities enable more effective handling of complex logical dependencies.*

6.2. Mechanism Analysis

We conduct two controlled experiments to explain why DART outperforms joint optimization by disentangling the effects of reasoning and tool-use.

Reasoning under Fixed Retrieval. We first examine whether *joint optimization degrades reasoning performance when retrieval quality is held fixed.* To this end, we force

DART to generate the final answers using identical retrieval contexts produced by the Search-R1 baseline, thereby **holding tool-use outputs fixed**. As shown in Figure 5, DART consistently outperforms Search-R1 under the same information inputs. Since retrieval quality is controlled, this performance gap suggests that joint optimization hinders effective learning of reasoning, whereas *DART maintains stronger reasoning capability via training-time isolation.* Moreover, in Appendix H.

DART vs. Hybrid Schemes. Next, we verify whether the *inference-time composition as in LEAS can match the improvement of DART.* To this end, We compare reasoning ability activated DART_{Reas} or tool-use ability activated DART_{Tool} with hybrid schemes (e.g., $\mathcal{H}_{\text{Tool}}$ in Section 4.2) that combine specialized models at inference time (Figure 1A). The empirical results in Table. 3 show that the DART with single ability substantially outperforms the corresponding hybrid baselines, further verifying that the *improvement brought by disentanglement* can not be replicated by inference-time hybrid schemes.

6.3. Ablation Study

Ablation 1: Effects of Disentangled LoRA Parameterization. We compare DART with representative single-LoRA and multi-agent baselines from Section 5 to analyze the effect of tool–reasoning parameterization.

Baselines. We consider the following baselines: (1) **Search-R1**, a standard single-model agent where tool-use and reasoning tokens are jointly optimized within a shared parameter space; (2) **LoRA**, which replaces full fine-tuning with

Table 2. Results on General QA and Multi-Hop QA datasets for **Qwen2.5-7b-Base/Instruct**. The best performance is set in bold. \diamond denotes results from (Jin et al., 2025). \dagger denotes in-domain datasets and $*$ denotes out-domain datasets.

Methods	General QA			Gen-Avg	Multi-Hop QA				MH-Avg	Avg
	NQ \dagger	TriviaQA*	PopQA*		HotpotQA \dagger	2Wiki*	Musique*	Bamboogle*		
Direct Inference \diamond	0.134	0.408	0.140	0.227	0.183	0.250	0.031	0.120	0.146	0.181
CoT \diamond	0.048	0.185	0.054	0.096	0.092	0.111	0.022	0.232	0.114	0.106
IRCoT \diamond	0.224	0.478	0.301	0.334	0.133	0.149	0.072	0.224	0.145	0.239
Search-o1 \diamond	0.151	0.443	0.131	0.242	0.187	0.176	0.062	0.296	0.180	0.206
RAG \diamond	0.349	0.585	0.392	0.442	0.299	0.235	0.058	0.208	0.200	0.304
SFT \diamond	0.318	0.354	0.121	0.264	0.217	0.259	0.066	0.112	0.164	0.207
R1-base \diamond	0.297	0.539	0.199	0.345	0.242	0.273	0.083	0.203	0.200	0.262
R1-instruct \diamond	0.270	0.537	0.199	0.335	0.237	0.292	0.072	0.293	0.224	0.271
Rejection Sampling \diamond	0.360	0.592	0.380	0.444	0.331	0.296	0.123	0.355	0.276	0.348
Search-R1-PPO-Base \diamond	0.480	0.638	0.457	0.525	0.433	0.382	0.196	0.432	0.361	0.431
Search-R1-PPO-Ins \diamond	0.393	0.610	0.397	0.467	0.370	0.414	0.146	0.368	0.325	0.385
Qwen2.5-7b-Instruct										
Search-R1-GRPO \diamond	0.429	0.623	0.427	0.493	0.386	0.346	0.162	0.400	0.324	0.396
DART	0.467	0.642	0.505	0.538	0.431	0.349	0.163	0.386	0.330	0.420
Qwen2.5-7b-Base										
Search-R1-GRPO \diamond	0.395	0.560	0.388	0.448	0.326	0.297	0.125	0.360	0.277	0.350
DART	0.472	0.639	0.507	0.539	0.425	0.338	0.155	0.376	0.323	0.416

Table 3. Comparison between DART with single ability and hybrid inference under isolated capability evaluation.

Methods	Qwen2.5-3B		Qwen2.5-7B	
	NQ	HotpotQA	NQ	HotpotQA
$\mathcal{H}_{\text{Reas}}$	0.435	0.324	0.438	0.327
DART _{Reas}	0.448	0.359	0.449	0.412
$\mathcal{H}_{\text{Tool}}$	0.248	0.212	0.305	0.255
DART _{Tool}	0.372	0.283	0.378	0.332

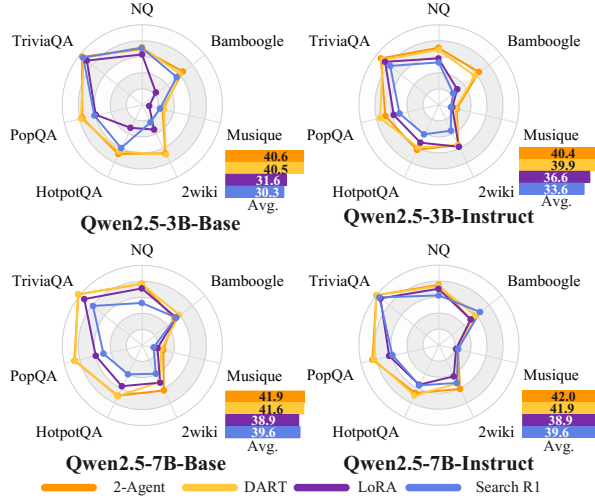


Figure 6. **DART recovers most of the benefits of the 2-Agent system within a single model.** Across model scales and benchmarks, DART consistently outperforms shared-parameter baselines and achieves performance comparable to the 2-Agent upper bound.

a single LoRA adapter ($r=16$) ¹, while still updating both

¹To make it a fair comparison, DART uses a single backbone with two disjoint LoRA subspaces ($r=8 \times 2$).

token types in the same low-rank subspace; **(3) 2-Agent**, a multi-agent system consisting of two independent models, one handling reasoning tokens and the other handling tool-use tokens (Figure 8), representing full parameter disentangled and serving as an upper bound.

Figure 6 reports results on Qwen2.5-3B/7B across multiple QA benchmarks. We observe three consistent patterns. **(1)** Vanilla LoRA performs nearly identically to Search-R1, and both fail to separate tool-use from reasoning, indicating that the bottleneck is not parameter capacity but interference arising from mixing different skills during training. **(2)** The 2-Agent baseline consistently achieves the strongest or near-strongest performance, confirming that *explicitly disentangling tool-use and reasoning parameters leads to improved results*. **(3)** DART closely approaches the performance of 2-Agent by enforcing gradient isolation within a single model, while avoiding the storage and deployment overhead of multi-agent systems. This observation is also consistent with prior findings in (Schulman & Lab, 2025).

Ablation 2: Effect of LoRA Rank. We further analyze the effect of the LoRA rank in DART and find that performance is largely insensitive to the rank choice; detailed results are reported in Appendix G.

7. Conclusion

This work proposes LEAS, an analysis framework that quantifies interference between tool-use and reasoning in ARL, revealing it as a fundamental optimization bottleneck. To mitigate this interference, we introduce DART, which iso-

lates tool-use and reasoning during training via two LoRA adapters. Extensive experiments show that explicitly disentangling these capabilities enables more effective optimization and consistently improves both reasoning and tool-use performance. This work provides insights for future research into multi-capabilities interactions in ARL.

Impact Statement

This work demonstrates that training-time disentanglement in DART mitigates optimization interference, thereby motivating further investigation into interactions among diverse capabilities and different tools during training. Such investigations may provide a principled path toward further improving the upper bound of agentic intelligence. There are many potential societal consequences of our work, none of which we feel must be specifically highlighted here.

References

Ahn, J., Verma, R., Lou, R., Liu, D., Zhang, R., and Yin, W. Large language models for mathematical reasoning: Progresses and challenges. In *European Chapter of the Association for Computational Linguistics*, 2024.

Bai, Y., Kadavath, S., Kundu, S., Askell, A., Kernion, J., Jones, A., Chen, A., Goldie, A., Mirhoseini, A., McKinnon, C., et al. Constitutional ai: Harmlessness from ai feedback. Preprint arXiv:2212.08073, 2022.

Chung, H. W., Hou, L., Longpre, S., Zoph, B., Tay, Y., Fedus, W., Li, Y., Wang, X., Dehghani, M., Brahma, S., et al. Scaling instruction-finetuned language models. *Journal of Machine Learning Research*, 2024.

Dong, G., Chen, Y., Li, X., Jin, J., Qian, H., Zhu, Y., Mao, H., Zhou, G., Dou, Z., and Wen, J.-R. Tool-star: Empowering llm-brained multi-tool reasoner via reinforcement learning. Preprint arXiv:2505.16410, 2025.

Feng, J., Huang, S., Qu, X., Zhang, G., Qin, Y., Zhong, B., Jiang, C., Chi, J., and Zhong, W. Retool: Reinforcement learning for strategic tool use in llms. Preprint arXiv:2504.11536, 2025.

Greene, W. H. *Econometric analysis*. Prentice Hall, 2003.

Guo, D., Yang, D., Zhang, H., Song, J., Zhang, R., Xu, R., Zhu, Q., Ma, S., Wang, P., Bi, X., et al. Deepseek-r1: Incentivizing reasoning capability in llms via reinforcement learning. Preprint arXiv:2501.12948, 2025.

Ho, X., Nguyen, A.-K. D., Sugawara, S., and Aizawa, A. Constructing a multi-hop qa dataset for comprehensive evaluation of reasoning steps. In *Proceedings of the 28th International Conference on Computational Linguistics*, 2020.

Hu, E. J., Wallis, P., Allen-Zhu, Z., Li, Y., Wang, S., Wang, L., Chen, W., et al. Lora: Low-rank adaptation of large language models. In *International Conference on Learning Representations*, 2022.

Huang, C., Liu, Q., Lin, B. Y., Pang, T., Du, C., and Lin, M. Lorahub: Efficient cross-task generalization via dynamic lora composition. In *First Conference on Language Modeling*, 2024.

Jiang, D., Lu, Y., Li, Z., Lyu, Z., Nie, P., Wang, H., Su, A., Chen, H., Zou, K., Du, C., et al. Verltool: Towards holistic agentic reinforcement learning with tool use. Preprint arXiv:2509.01055, 2025.

Jin, B., Zeng, H., Yue, Z., Yoon, J., Arik, S. O., Wang, D., Zamani, H., and Han, J. Search-r1: Training LLMs to reason and leverage search engines with reinforcement learning. In *Second Conference on Language Modeling*, 2025.

Joshi, M., Choi, E., Weld, D. S., and Zettlemoyer, L. Triviaqa: A large scale distantly supervised challenge dataset for reading comprehension. In *Association for Computational Linguistics*, 2017.

Karpukhin, V., Oguz, B., Min, S., Lewis, P., Wu, L., Edunov, S., Chen, D., and Yih, W.-t. Dense passage retrieval for open-domain question answering. In *Empirical Methods in Natural Language Processing*, 2020.

Kwiatkowski, T., Palomaki, J., Redfield, O., Collins, M., Parikh, A., Alberti, C., Epstein, D., Polosukhin, I., Devlin, J., Lee, K., et al. Natural questions: a benchmark for question answering research. *Transactions of the Association for Computational Linguistics*, 2019.

Lewis, P., Perez, E., Piktus, A., Petroni, F., Karpukhin, V., Goyal, N., Küttler, H., Lewis, M., Yih, W.-t., Rocktäschel, T., et al. Retrieval-augmented generation for knowledge-intensive nlp tasks. *Conference on Neural Information Processing Systems*, 2020.

Li, D., Ma, Y., Wang, N., Ye, Z., Cheng, Z., Tang, Y., Zhang, Y., Duan, L., Zuo, J., Yang, C., et al. Mixlora: Enhancing large language models fine-tuning with lora-based mixture of experts. Preprint arXiv:2404.15159, 2024.

Li, K., Zhang, Z., Yin, H., Ye, R., Zhao, Y., Zhang, L., Ou, L., Zhang, D., Wu, X., Wu, J., et al. Websailor-v2: Bridging the chasm to proprietary agents via synthetic data and scalable reinforcement learning. Preprint arXiv:2509.13305, 2025a.

Li, X., Dong, G., Jin, J., Zhang, Y., Zhou, Y., Zhu, Y., Zhang, P., and Dou, Z. Search-o1: Agentic search-enhanced large reasoning models. Preprint arXiv:2501.05366, 2025b.

Li, Z., Yi, M., Wang, Y., Cui, S., and Liu, Y. Towards a theoretical understanding to the generalization of rlhf. Preprint arXiv:2601.16403, 2026.

Luo, S., Yang, H., Xin, Y., Yi, M., Wu, G., Zhai, G., and Liu, X. Tr-pt: Task-relevant parameter and token selection for efficient tuning. In *International Conference on Computer Vision*, 2025.

Luo, T., Lei, J., Lei, F., Liu, W., He, S., Zhao, J., and Liu, K. Moelora: Contrastive learning guided mixture of experts on parameter-efficient fine-tuning for large language models. Preprint arXiv:2402.12851, 2024.

Ma, Y., Liang, Z., Dai, H., Chen, B., Gao, D., Ran, Z., Zihan, W., Jin, L., Jiang, W., Zhang, G., et al. Modula: Mixture of domain-specific and universal lora for multi-task learning. In *Empirical Methods in Natural Language Processing*, 2024.

Mai, X., Xu, H., W, X., Wang, W., Zhang, Y., and Zhang, W. Agentic RL scaling law: Spontaneous code execution for mathematical problem solving. In *Conference on Neural Information Processing Systems*, 2025.

Mallen, A., Asai, A., Zhong, V., Das, R., Hajishirzi, H., and Khashabi, D. When not to trust language models: Investigating effectiveness and limitations of parametric and non-parametric memories. Preprint arXiv:2212.10511, 2022.

Mukherjee, S., Yuan, L., Hakkani-Tür, D., and Peng, H. Reinforcement learning finetunes small subnetworks in large language models. In *Conference on Neural Information Processing Systems*, 2025.

Ouyang, L., Wu, J., Jiang, X., Almeida, D., Wainwright, C., Mishkin, P., Zhang, C., Agarwal, S., Slama, K., Ray, A., et al. Training language models to follow instructions with human feedback. *Conference on Neural Information Processing Systems*, 2022.

Peiyuan, F., He, Y., Huang, G., Lin, Y., Zhang, H., Zhang, Y., and Li, H. Agile: A novel reinforcement learning framework of llm agents. *Conference on Neural Information Processing Systems*, 2024.

Press, O., Zhang, M., Min, S., Schmidt, L., Smith, N. A., and Lewis, M. Measuring and narrowing the compositionality gap in language models. In *Findings of the Association for Computational Linguistics: EMNLP 2023*, 2023.

Qian, C., Acikgoz, E. C., He, Q., Wang, H., Chen, X., Hakkani-Tür, D., Tur, G., and Ji, H. Toolrl: Reward is all tool learning needs. Preprint arXiv:2504.13958, 2025.

Qiao, Z., Chen, G., Chen, X., Yu, D., Yin, W., Wang, X., Zhang, Z., Li, B., Yin, H., Li, K., et al. Webresearcher: Unleashing unbounded reasoning capability in long-horizon agents. Preprint arXiv:2509.13309, 2025.

Ren, Y. and Sutherland, D. J. Learning dynamics of llm finetuning. In *International Conference on Learning Representations*, 2025.

Schick, T., Dwivedi-Yu, J., Dessì, R., Raileanu, R., Lomeli, M., Hambro, E., Zettlemoyer, L., Cancedda, N., and Scialom, T. Toolformer: Language models can teach themselves to use tools. *Conference on Neural Information Processing Systems*, 2023.

Schulman, J. and Lab, T. M. Lora without regret. *Thinking Machines Lab: Connectionism*, 2025.

Shao, Z., Wang, P., Zhu, Q., Xu, R., Song, J., Bi, X., Zhang, H., Zhang, M., Li, Y., et al. Deepseekmath: Pushing the limits of mathematical reasoning in open language models. Preprint arXiv:2402.03300, 2024.

Sheng, G., Zhang, C., Ye, Z., Wu, X., Zhang, W., Zhang, R., Peng, Y., Lin, H., and Wu, C. Hybridflow: A flexible and efficient rlhf framework. In *European Conference on Computer Systems*, 2025.

Singh, J., Magazine, R., Pandya, Y., and Nambi, A. Agentic reasoning and tool integration for llms via reinforcement learning. Preprint arXiv:2505.01441, 2025.

Su, L., Zhang, Z., Li, G., Chen, Z., Wang, C., Song, M., Wang, X., Li, K., Wu, J., Chen, X., et al. Scaling agents via continual pre-training. Preprint arXiv:2509.13310, 2025.

Team, Q. Qwen2 technical report. Preprint arXiv:2407.10671, 2024.

Trivedi, H., Balasubramanian, N., Khot, T., and Sabharwal, A. Musique: Multi-hop questions via single-hop question composition. *Transactions of the Association for Computational Linguistics*, 2022.

Trivedi, H., Balasubramanian, N., Khot, T., and Sabharwal, A. Interleaving retrieval with chain-of-thought reasoning for knowledge-intensive multi-step questions. In *Proceedings of the 61st annual meeting of the association for computational linguistics*, 2023.

Wang, H., Sun, T., Jin, C., Wang, Y., Fan, Y., Xu, Y., Du, Y., and Fan, C. Customizable combination of parameter-efficient modules for multi-task learning. In *International Conference on Learning Representations*, 2024.

Wang, L., Yang, N., Huang, X., Jiao, B., Yang, L., Jiang, D., Majumder, R., and Wei, F. Text embeddings by

weakly-supervised contrastive pre-training. Preprint arXiv:2212.03533, 2022.

Wei, J., Wang, X., Schuurmans, D., Bosma, M., Xia, F., Chi, E., Le, Q. V., Zhou, D., et al. Chain-of-thought prompting elicits reasoning in large language models. *Conference on Neural Information Processing Systems*, 2022.

Wei, Y., Yu, X., Weng, Y., Pan, T., Li, A., and Du, L. Autotir: Autonomous tools integrated reasoning via reinforcement learning. Preprint arXiv:2507.21836, 2025.

Wu, S., Zhao, S., Huang, Q., Huang, K., Yasunaga, M., Cao, K., Ioannidis, V., Subbian, K., Leskovec, J., and Zou, J. Y. Avatar: Optimizing llm agents for tool usage via contrastive reasoning. *Conference on Neural Information Processing Systems*, 2024.

Wu, W., Guan, X., Huang, S., Jiang, Y., Xie, P., Huang, F., Cao, J., Zhao, H., and Zhou, J. Masksearch: A universal pre-training framework to enhance agentic search capability. Preprint arXiv:2505.20285, 2025a.

Wu, X., Huang, S., and Wei, F. Mixture of lora experts. In *International Conference on Learning Representations*, 2025b.

Yang, Z., Qi, P., Zhang, S., Bengio, Y., Cohen, W., Salakhutdinov, R., and Manning, C. D. Hotpotqa: A dataset for diverse, explainable multi-hop question answering. In *Conference on Empirical Methods in Natural Language Processing*, 2018.

Yu, T., Kumar, S., Gupta, A., Levine, S., Hausman, K., and Finn, C. Gradient surgery for multi-task learning. *Conference on Neural Information Processing Systems*, 2020.

Yu, Y., Ping, W., Liu, Z., Wang, B., You, J., Zhang, C., Shoeybi, M., and Catanzaro, B. Rankrag: Unifying context ranking with retrieval-augmented generation in llms. *Conference on Neural Information Processing Systems*, 2024.

Zeng, A., Liu, M., Lu, R., Wang, B., Liu, X., Dong, Y., and Tang, J. Agenttuning: Enabling generalized agent abilities for llms. In *Findings of the Association for Computational Linguistics*, 2024.

Zhang, S., Fan, J., Fan, M., Li, G., and Du, X. Deepanalyze: Agentic large language models for autonomous data science. Preprint arXiv:2510.16872, 2025a.

Zhang, Y., Fan, M., Fan, J., Yi, M., Luo, Y., Tan, J., and Li, G. Reward-sql: Boosting text-to-sql via step-wise reasoning and process-supervised rewards. Preprint arXiv:2505.04671, 2025b.

Zhu, Y., Wickers, N., Lin, C.-C., Wang, X., Chen, T., Shu, L., Lu, H., Liu, C., Luo, L., Chen, J., et al. Sira: Sparse mixture of low rank adaptation. Preprint arXiv:2311.09179, 2023.

A. Formulation of ARL

In the main text, we present a simplified policy gradient formulation (Eq. (2)) to focus on the interaction between reasoning and tool-use tokens. In practice, following standard RLHF and agentic RL setups, policy optimization additionally incorporates a KL-divergence regularization term to constrain the learned policy from drifting excessively from a reference policy.

Concretely, let π_θ denote the current policy and π_{ref} the reference policy (initialized from the pretrained model). The regularized objective is given by:

$$\mathcal{J}(\theta) = \mathbb{E}_{\tau \sim \pi_\theta} [R(\tau) - \beta \text{KL}(\pi_\theta(\cdot | c_{<t}) \| \pi_{\text{ref}}(\cdot | c_{<t}))], \quad (11)$$

where β controls the strength of the KL regularization.

Under this objective, the policy gradient can be written as:

$$\nabla_\theta \mathcal{J}(\theta) \approx \mathbb{E}_{\tau \sim \pi_\theta} \left[\sum_{t=1}^T \left(A(\tau) - \beta \log \frac{\pi_\theta(c_t | c_{<t})}{\pi_{\text{ref}}(c_t | c_{<t})} \right) \nabla_\theta \log \pi_\theta(c_t | c_{<t}) \right]. \quad (12)$$

This formulation shows that the KL term acts as an additional token-level penalty that discourages large deviations from the reference policy during training. Throughout this work, we omit the KL term in the main exposition for clarity, as it does not affect the proposed token-level gradient isolation or the analysis of capability interference. All experiments are conducted with KL regularization enabled, using a fixed coefficient β as reported in Appendix B.

B. Experimental Settings

This section details the experimental settings used in our RL training, including the training algorithm, rollout configuration, prompt template, reward formulation, and system-level optimizations. Unless otherwise stated, these settings are shared across all experiments.

B.1. RL Training Setup

For GRPO training, we follow the implementation in Verl (Sheng et al., 2025). The backbone model is Qwen2.5 (Team, 2024) series integrates a retrieval tool. We use an E5 retriever (Wang et al., 2022) and the 2018 Wikipedia dump (Karpukhin et al., 2020) as the corpus. All experiments are conducted on a cluster of $8 \times$ NVIDIA A800 GPUs. Training is conducted for 100 optimization steps with a learning-rate warm-up ratio of 0.1. All GRPO experiments use a fixed configuration with rollout batch size 256, gradient batch size 64, temperature 1.0, top- p 1.0, and learning rate 1×10^{-6} . The rollout temperature and top- p are both fixed to 1.0. The KL-divergence coefficient β and clipping ratio ϵ are set to 0.001 and 0.2, respectively.

For all variants involving LoRA adaptation, we scale the learning rate by $10 \times$ following prior guidance (Schulman & Lab, 2025). To enable precise token-level routing in DART, we extend the tokenizer vocabulary with a small set of special tokens that explicitly mark reasoning and tool-use segments.

To improve training efficiency, we enable gradient checkpointing, FSDP offloading, and vLLM-based rollouts.

Model checkpoints are saved every 20 training steps. If training diverges, we evaluate the most recent stable checkpoint according to the reward curve; otherwise, the final checkpoint is used for evaluation. The maximum action budget B is set to 4, and the top 3 retrieved passages are used by default.

Overall, this unified setup ensures that *observed differences are attributable to the parameterization and routing design*, rather than changes in data, tools, or optimization settings.

B.2. Prompt Template

Following Search-R1 (Jin et al., 2025), we use same prompt template that enforces a minimal structural format while avoiding content-specific biases. As illustrated in Table 4, the template structures the model output into three iterative stages: (1) a reasoning phase, (2) a search engine invocation phase, and (3) a final answer.

Importantly, we intentionally restrict the constraints to this high-level structure, without enforcing reflective reasoning styles, specific search strategies, or problem-solving heuristics. This design choice ensures that the model’s learning dynamics

during RL remain observable and unbiased, allowing behaviors to emerge naturally from optimization rather than prompt engineering.

Prompt Template

Answer the given question. You must conduct reasoning inside `<think>` and `</think>` first every time you get new information. After reasoning, if you find you lack some knowledge, you can call a search engine by `<search>` query `</search>`, and it will return the top searched results between `<information>` and `</information>`. You can search as many times as you want. If you find no further external knowledge needed, you can directly provide the answer inside `<answer>` and `</answer>` without detailed illustrations. For example, `<answer> xxx </answer>`. Question: question.

Table 4. Prompt template in this paper. The placeholder question is replaced with the specific query during both training and inference.

B.3. Reward Function

The reward function serves as the sole training signal in our RL framework. We adopt a rule-based outcome reward that evaluates the correctness of the model’s final answer, without incorporating intermediate or format-based rewards. Specifically, for factual reasoning tasks, the reward is computed using exact match (EM):

$$r_\phi(x, y) = \text{EM}(a_{\text{pred}}, a_{\text{gold}}), \quad (13)$$

where a_{pred} is the extracted final answer from the model response y , and a_{gold} denotes the ground-truth answer.

C. Mathematical Intuition of LEAS

In this paper, we consider three base capabilities of LLM, represented by base x_1 , tool-using x_2 , and reasoning x_3 , together with their pairwise interaction indicators x_{12}, x_{13}, x_{23} . For a given question q , LEAS models the logit of correctness as

$$z_{\mathcal{M}}^q = \mathbf{x}_{\mathcal{M}}^\top \boldsymbol{\lambda}^q, \quad \boldsymbol{\lambda}^q = [\lambda_1^q, \lambda_2^q, \lambda_3^q, \lambda_{12}^q, \lambda_{13}^q, \lambda_{23}^q]. \quad (14)$$

To interpret the interaction coefficient λ_{23}^q between tool use and reasoning, we form a contrast over four model configurations that differ only in whether tool-use and reasoning are jointly optimized, while keeping the base capability active ($x_1 = 1$):

- **Unified model:** $\mathbf{x}_{\text{Uni}} = [1, 1, 1, 1, 1, 1]$,
- **Tool-specialized model:** $\mathbf{x}_{\text{Tool}} = [1, 1, 0, 1, 0, 0]$,
- **Reasoning-specialized model:** $\mathbf{x}_{\text{Reas}} = [1, 0, 1, 0, 1, 0]$,
- **Base model:** $\mathbf{x}_{\text{Base}} = [1, 0, 0, 0, 0, 0]$.

Plugging these indicator vectors into $z_{\mathcal{M}}^q = \mathbf{x}_{\mathcal{M}}^\top \boldsymbol{\lambda}^q$, we obtain

$$z_{\text{Uni}}^q = \lambda_1^q + \lambda_2^q + \lambda_3^q + \lambda_{12}^q + \lambda_{13}^q + \lambda_{23}^q, \quad (15)$$

$$z_{\text{Tool}}^q = \lambda_1^q + \lambda_2^q + \lambda_{12}^q, \quad (16)$$

$$z_{\text{Reas}}^q = \lambda_1^q + \lambda_3^q + \lambda_{13}^q, \quad (17)$$

$$z_{\text{Base}}^q = \lambda_1^q. \quad (18)$$

Therefore, the following contrast isolates the tool–reasoning interaction term:

$$\lambda_{23}^q = z_{\text{Uni}}^q - z_{\text{Tool}}^q - z_{\text{Reas}}^q + z_{\text{Base}}^q. \quad (19)$$

Intuitively, we can interpret this by grouping the terms as the joint improvement versus the sum of individual improvements:

$$\lambda_{23}^q = (z_{\text{Uni}}^q - z_{\text{Base}}^q) - [(z_{\text{Tool}}^q - z_{\text{Base}}^q) + (z_{\text{Reas}}^q - z_{\text{Base}}^q)]. \quad (20)$$

The first part represents the total performance leap when tool-use and reasoning are optimized together. The second part represents the theoretical sum of performance gains if each capability were developed in isolation. Notably, in this setting, the “disentangled” reasoning and tool-using group is artificially constructed which is nonexistent in practice. In contrast, our DART, naturally disentangles tool-using and reasoning i.e., corresponding $\lambda_{23} = 0$.

D. Experimental Details for Reasoning–Tool Interaction Analysis

This section provides additional experimental details for the reasoning–tool interaction analysis shown in Figure 2. We instantiate LEAS on the NQ and HotpotQA datasets to estimate the question-level interaction coefficient λ_{23}^q . At evaluation time, we assess each model–question pair via repeated stochastic decoding and measure correctness using exact match (EM). Formally, for a model \mathcal{M} and a question q , let $\{a_q^{(n)}\}_{n=1}^N$ denote N decoded answers generated under non-deterministic sampling. The empirical correctness is defined as

$$\hat{s}_{\mathcal{M}}^q = \frac{1}{N} \sum_{n=1}^N \text{EM}(a_q^{(n)}, a_{\text{gold}}),$$

where $\text{EM}(\cdot) \in \{0, 1\}$. In all experiments, we set $N = 50$ and adopt the same stochastic decoding strategy as Appendix B, with fixed temperature and top- p sampling. Averaging over multiple samples reduces decoding noise and yields a more stable estimate of model correctness.

For each question q , we consider the six models defined in Section 4.1, which correspond to different combinations of base, tool-use, and reasoning capabilities and induce a fixed design matrix \mathbf{X} . All models are trained under identical hyper-parameters and to convergence, *differing only in capability activation*, which ensures controlled and fair comparisons across models. Given the six empirical correctness estimates $\{\hat{s}_{\mathcal{M}}^q\}$, we solve a linear system in logit space to obtain the question-level effect vector λ^q . The interaction coefficient λ_{23}^q captures the deviation of the jointly optimized reasoning–tool-use configuration from the linear additive expectation of the two individual capabilities, where negative values indicate interference and positive values indicate synergy.

For statistical analysis, we retain only questions for which at least one of the six models produces a correct prediction. We then aggregate λ_{23}^q across all retained questions and report the proportion of negative and positive values. To analyze the relationship between interaction patterns and task solvability, we further bin questions by λ_{23}^q and compute the average correctness within each bin, producing the histograms and overlaid curves shown in Figure 2. All analyses are conducted with both Qwen2.5-3B and Qwen2.5-7B models on NQ and HotpotQA, verifying that the observed interaction patterns are consistent across model capacities and task difficulties. Except for the statistical procedures described above, all inference and evaluation hyper-parameters follow the settings of the main experiments.

E. Implementation Details of Gradient Conflict

This section provides implementation details for the gradient angle analysis described in the main text. Following the training and sampling protocol of (Jin et al., 2025), for each input query we sample $N = 16$ rollouts $\{\tau_i\}_{i=1}^N$ from the current policy. All analyses are conducted with fixed base model parameters: we perform forward and backward passes solely to extract gradients and do not update the model.

Based on the token-level masked update in Eq. 8 and the hyperparameter settings described in Appendix B, we compute policy gradients for different token roles within each trajectory. Specifically, for each rollout τ_i , we compute gradients $\mathbf{g}_{\tau_i}^{(b)}$ for token role $b \in \{r, a\}$, where r denotes reasoning tokens and a denotes tool-use tokens. Gradients for different roles are obtained via separate backward passes, with gradients explicitly zeroed between passes to avoid accumulation effects.

Gradient angles are computed from the cosine similarity between two gradient vectors. Given two gradients \mathbf{g}_1 and \mathbf{g}_2 , we first compute their cosine similarity as

$$\cos(\mathbf{g}_1, \mathbf{g}_2) = \frac{\mathbf{g}_1^\top \mathbf{g}_2}{\|\mathbf{g}_1\|_2 \|\mathbf{g}_2\|_2},$$

where gradients are flattened over all model parameters. The corresponding angle is then obtained by

$$\angle(\mathbf{g}_1, \mathbf{g}_2) = \arccos(\cos(\mathbf{g}_1, \mathbf{g}_2)),$$

which yields values in $[0, \pi]$. This conversion allows us to interpret gradient alignment geometrically, with smaller angles indicating stronger alignment and angles approaching $\pi/2$ or larger indicating increasing degrees of misalignment.

All experiments use the same numerical and system settings as training. We enable FlashAttention-2 and gradient checkpointing to support long-sequence computation, and perform all forward and backward passes in bfloat16 precision. In

memory-constrained environments, parameters are managed with CPU offloading. The maximum lengths of both prompts and responses are set to 4096 tokens.

Notably, all gradients are computed over the full sequence, but only tokens selected by the corresponding role mask contribute to the policy loss and backpropagation. Gradient clipping is disabled by default to avoid altering the geometry of gradients. We additionally observe qualitatively similar gradient angle patterns when repeating the analysis at other training steps, suggesting that the observed gradient conflict is not specific to a single checkpoint.

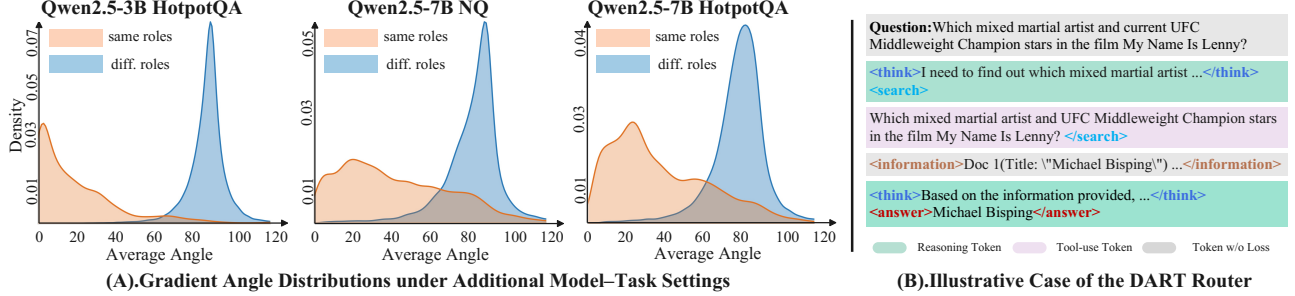


Figure 7. Gradient Misalignment and Router Behavior in DART. (A). Gradient angle distributions under additional model–task settings, showing that gradients from the same capability are well aligned, while gradients between reasoning and tool-use tokens are largely orthogonal. (B). An illustrative example of the DART router, highlighting **rule-based** token-level routing decisions that distinguish reasoning, tool-use, and loss-free tokens during a tool-augmented QA process.

Figure 7(A) shows that across all settings, reasoning–tool gradients are close to orthogonal, while same-capability gradients exhibit stronger alignment, indicating clear directional separation. Compared to the 3B model, the 7B model shows a more dispersed distribution of same-role gradients, which we attribute to its larger capacity: with more parameters, the model admits a wider range of gradient directions for the same capability across different samples.

F. Theoretical Efficiency: DART vs. 2-Agent System

A common alternative to a unified model is a disentangled 2-agent system, where a specialized reasoning model $\mathcal{M}_{\text{Reas}}$ and a tool-use model $\mathcal{M}_{\text{Tool}}$ collaborate. While this modularity seems intuitive, it introduces significant overhead in resource consumption and latency. Below, we provide a theoretical analysis of why the DART framework is more efficient.

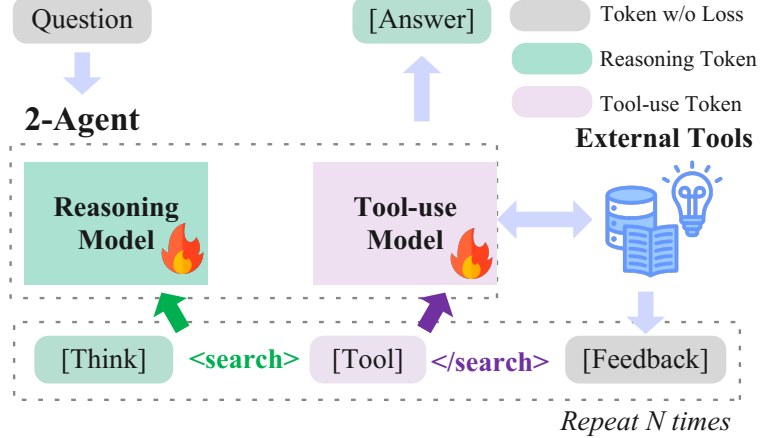


Figure 8. 2-Agent System Architecture. A reasoning model and a tool-use model operate as separate models and interact through explicit handoffs. The reasoning model decides when to invoke tools, while the tool-use model executes tool calls and returns feedback.

Training Memory: The Shared-Backbone Advantage We analyze the training-time GPU memory complexity of DART in comparison with 2-agent system. Let P denote the number of parameters in the backbone model, and let p denote the number of parameters introduced by a LoRA adapter, where $p \ll P$ (typically below 0.5% of P). Model parameters and gradients are stored in BF16 precision, while optimizer states are stored in FP32 precision.

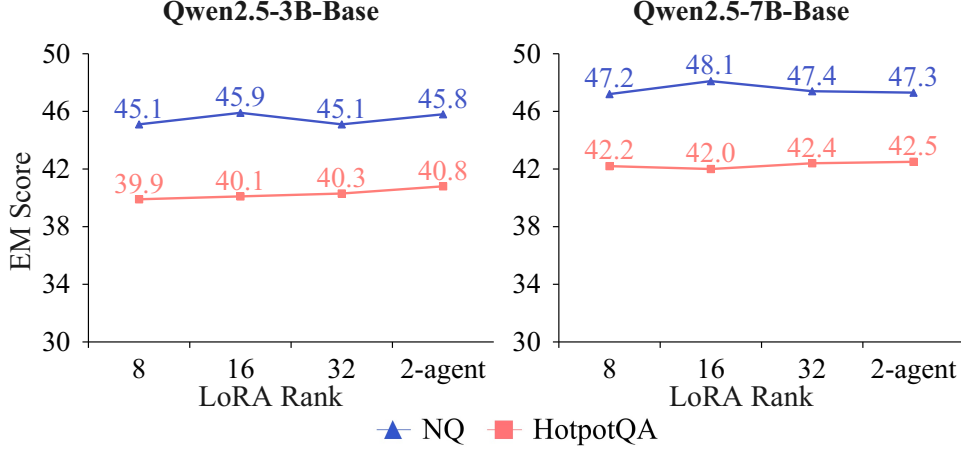


Figure 9. **LoRA Rank Sensitivity.** DART exhibits stable EM performance across LoRA ranks and remains close to the 2-agent baseline.

Metric	disentangled 2-Agent (LoRA)	DART (Multi-LoRA)
Backbone Instances	2	1
VRAM (Weight-dominant)	$\approx 2P$	$\approx 1P$
Context Switching Cost	High (Re-encoding $\mathcal{O}(L^2)$)	Zero (KV-Cache Reuse)

Table 5. Theoretical comparison between a disentangled 2-agent system and the DART framework. P denotes the backbone parameter count; L denotes sequence length.

Under a disentangled multi-agent GRPO setup, two trainable policy backbone models must be resident on GPU. For each model, training stores parameters, gradients, and Adam-style optimizer states, contributing approximately parameters. As a result, the dominant static memory cost scales as $\mathcal{O}(P_{2\text{-agent}} \approx 2 \times 4P = 8P)$. In contrast, DART trains both capabilities within a single shared backbone and confines all trainable parameters to lightweight LoRA adapters. The backbone is frozen, and gradients as well as optimizer states are stored only for the adapter parameters. As a result, the dominant static memory cost scales as $\mathcal{O}(P_{\text{DART}}) \approx P + \mathcal{O}(p)$, where the contribution of p is negligible.

According to our empirical observation, the resulting memory ratio can be approximated as

$$\frac{\mathcal{O}(P_{2\text{-agent}})}{\mathcal{O}(P_{\text{DART}})} \approx \mathcal{O}(8).$$

DART reduces the training-time static memory footprint by roughly $8\times$ while maintaining performance comparable to 2-agent.

Inference Latency: The KV-Cache Advantage. The most critical bottleneck in multi-turn interactions is computing the prefill during context switching.

- **2-Agent Latency:** When $\mathcal{M}_{\text{Reas}}$ generates a thought and hands it to $\mathcal{M}_{\text{Tool}}$, the latter must re-encode the entire conversation history H of length L to build its own Key-Value (KV) cache. This re-computation has a complexity of $\mathcal{O}(L^2)$.
- **DART Latency:** Since DART operates on a single backbone, the KV-cache remains valid across capability switches. Moving from reasoning to tool-invocation only requires a negligible $\mathcal{O}(1)$ switch of the active LoRA ranks. The historical context is never re-processed, drastically reducing the Time-To-First-Token (TTFT) for subsequent turns.

As summarized in Table 5, DART simplifies the deployment stack. A 2-agent system requires an external orchestrator to synchronize states and format prompts between models, whereas DART internalizes this logic within a single inference pipeline.

G. Effect of LoRA Rank in DART

We study the effect of the LoRA rank in DART by varying the adapter rank on the **Qwen2.5-3B-Base** model. Figure. 10(A) reports DART’s EM performance on NQ and HotpotQA under different LoRA ranks (8/16/32) for both Qwen2.5-3B and Qwen2.5-7B backbones, with the 2-agent system shown as a reference. Overall, **DART is not strongly sensitive to the rank choice**: varying the rank changes EM only marginally, and the relative ordering across datasets and model scales remains consistent. Across all settings, DART stays close to the 2-agent baseline, indicating that *its improvements are not driven by simply increasing adapter capacity*. This is an interesting observation, which indicates that under the disentangled learning paradigm, a slight parameter capacity is enough to make the model complete the task well in practice.

H. Retrieval Accuracy Evaluation

In section 6.2, we show that the single ability of DART is also improved, compared to the hybrid model. Next, we directly verify the search accuracy of DART model is improved, compared with baseline model. Concretely, we report the retrieval accuracy results and the corresponding evaluation protocol, which are presented exclusively here to analyze tool-use behavior under different training paradigms. We compare the jointly trained Search-R1 baseline with DART on the NQ and HotpotQA benchmarks, focusing on the model’s ability to retrieve task-relevant information during inference.

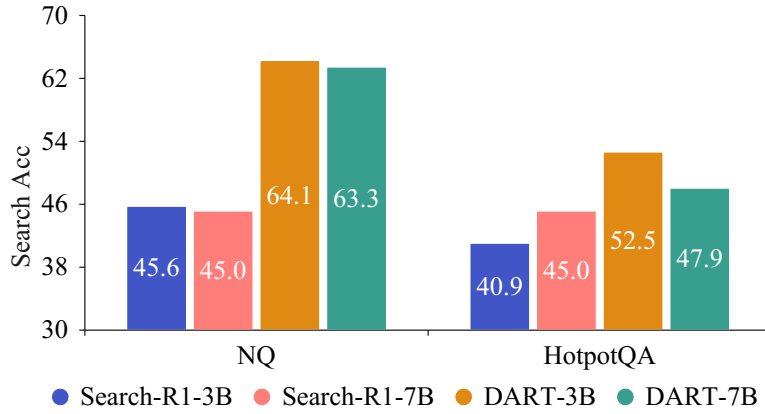


Figure 10. **Search Accuracy of DART.** DART achieves higher search accuracy than Search-R1 on both NQ and HotpotQA, showing that DART consistently achieves higher search accuracy across both datasets and model scales.

We evaluate retrieval performance using *retrieval accuracy*. Let \mathcal{S} denote the evaluation set. For each example $j \in \mathcal{S}$, the model retrieves a set of information documents or passages denoted by \mathcal{D}_j , and the ground-truth answer set is given by G_j . We define a retrieval correctness indicator $\text{RetCorrect}(\mathcal{D}_j, G_j)$, which equals 1 if there exists at least one retrieved document in \mathcal{D}_j that matches any element in G_j , and 0 otherwise. The overall retrieval accuracy is then defined as

$$\text{Acc} = \frac{1}{|\mathcal{S}|} \sum_{j \in \mathcal{S}} \text{RetCorrect}(\mathcal{D}_j, G_j).$$

We report retrieval accuracy for both Qwen2.5-3B and Qwen2.5-7B backbones under identical data splits and inference settings. Search-R1 optimizes reasoning and tool use jointly, whereas DART isolates their parameter updates during training. All methods share the same retrieval format and correctness criterion.

As shown in Figure 10(B), DART consistently achieves higher retrieval accuracy than Search-R1 across both datasets and model scales. This indicates that DART retrieves task-relevant information more reliably, particularly on multi-hop and fact-intensive tasks, highlighting the effectiveness of training-time capability disentanglement for tool use.

In the results, we observe an interesting phenomenon. For our DART, the 7B model does not consistently outperform 3B model in retrieval accuracy. This introduce an open problem says that selecting the proper size of backbone model to invoke tools significantly improves the final overall performance. We leave the exploration to this as the future work.